Earth and Planetary Science Letters 410 (2015) 84–96

Contents lists available at ScienceDirect

Earth and Planetary Science Letters

www.elsevier.com/locate/epsl

Cadmium-isotopic evidence for increasing primary productivity during the Late Permian anoxic event

Svetoslav V. Georgiev [a,*], Tristan J. Horner [b,1], Holly J. Stein [a,c], Judith L. Hannah [a,c], Bernard Bingen [d], Mark Rehkämper [e]

[a] AIRIE Program, Colorado State University, Fort Collins, CO 80523-1482, USA
[b] Department of Earth Sciences, University of Oxford, OX1 3AN, UK
[c] Centre for Earth Evolution and Dynamics, University of Oslo, 0316 Oslo, Norway
[d] Geological Survey of Norway, 7491 Trondheim, Norway
[e] Department of Earth Science and Engineering, Imperial College London, SW7 2AZ, UK

ARTICLE INFO

Article history:
Received 10 July 2014
Received in revised form 16 October 2014
Accepted 7 November 2014
Available online xxxx
Editor: J. Lynch-Stieglitz

Keywords:
cadmium isotopes
productivity
anoxia
upwelling
shale

ABSTRACT

Earth's most extreme extinction event near the end of the Late Permian decimated more than 90% of all extant marine species. Widespread and intensive oceanic anoxia almost certainly contributed to the catastrophe, though the driving mechanisms that sustained such conditions are still debated. Of particular interest is whether water column anoxia was a consequence of a 'stagnant ocean', or if it was controlled by increases in nutrient supply, primary productivity, and subsequent heterotrophic respiration. Testing these competing hypotheses requires deconvolving sedimentary/bottom water redox conditions from changes in surface water productivity in marine sediments. We address this issue by studying marine shales from East Greenland and the mid-Norwegian shelf and combining sedimentary redox proxies with cadmium-isotopic analyses. Sedimentary nitrogen-isotopic data, pyrite framboid analyses, and organic and inorganic shale geochemistry reveal sulfidic conditions with vigorous upwelling, and increasingly anoxic conditions with a strengthening upwelling in the Greenland and Norwegian sections, respectively. Detailed analysis of sedimentary metal budgets illustrates that Cd is primarily associated with organic carbon and records primary geochemical signatures, thus enabling reconstruction of surface water nutrient utilization. Cadmium-isotopic analyses of the authigenic shale fraction released by *inverse aqua regia* digestion yield an average $\delta^{114/110}$Cd of $+0.15 \pm 0.01$‰ (2 SE, $n = 12$; rel. NIST SRM 3108), indicative of incomplete surface water nutrient utilization up-section. The constant degree of nutrient utilization combined with strong upwelling requires increasing primary productivity – and not oceanic stagnation – to balance the larger nutrient fluxes to both study sites during the development of the Late Permian water column anoxia. Overall, our data illustrate that if bottom water redox and upwelling can be adequately constrained, Cd-isotopic analyses of organic-rich sediments can be used to provide valuable information on nutrient utilization and therefore past productivity.

1. Introduction

Exceptionally widespread oceanic anoxia is widely considered one of the main contributing factors to the Late Permian marine biotic extinction (e.g., Isozaki, 1997; Wignall and Twitchett, 2002a; Bond and Wignall, 2010). Oxygen deficiency was already widespread in the pre-extinction Late Permian oceans, with possible sulfidic conditions developing in mid-water column depths that reached some surface waters (e.g., Algeo et al., 2010; Brennecka et al., 2011). Further expansion and development of peak anoxic conditions coincided with the main biotic extinction (Brennecka et al., 2011), which decimated most marine taxa ~251.9 Ma ago (Burgess et al., 2014).

The mechanisms that formed, expanded and sustained the Late Permian anoxia are still debated, but are generally thought to be related to either a more sluggish oceanic circulation, or an increase in marine primary productivity (and associated heterotrophy) in response to greater oceanic upwelling. A general slowdown in oceanic circulation is consistent with the decreased latitudinal temperature gradients of the Late Permian greenhouse world (e.g., Isozaki, 1997). Such conditions were likely triggered/sustained by

* Corresponding author.
E-mail address: georgiev@colostate.edu (S.V. Georgiev).
[1] Now at: Department of Marine Chemistry and Geochemistry, Woods Hole Oceanographic Institution, Woods Hole, MA 02543-1050, USA.

http://dx.doi.org/10.1016/j.epsl.2014.11.010
0012-821X/

the injection of substantial greenhouse gas emissions associated with the eruption of the Siberian Trap basalts (e.g., Wignall and Twitchett, 2002a). Alternatively, increased upwelling and biological mechanisms have been hypothesized to contribute to the anoxia (e.g., Algeo et al., 2010; Meyer et al., 2011). A particular focus has been on the oxygen consuming feedback associated with increased upwelling, primary productivity, and subsequent heterotrophy (e.g., Wyrtki, 1962). However, distinguishing between the stagnation and upwelling hypotheses requires proxies that can discriminate nutrient supply from nutrient utilization (i.e. the amount of nutrient available and the fraction of nutrients that are consumed, respectively). The marine geochemistry of Cd (cadmium) offers a potential solution to this problem.

Cadmium is a post-transition metal that is actively cycled by marine microbes in the water column (e.g., Sunda, 2012). Dissolved cadmium in seawater has a nutrient-like distribution that follows – albeit with some scatter – that of dissolved inorganic PO_4^{3-} (phosphate; e.g., Boyle et al., 1976; Cullen, 2006; Hendry et al., 2008). Microbial Cd uptake efficiently removes most dissolved Cd from surface waters, where it is exported to the deep ocean and seafloor in the form of particulate organic matter (OM). As this OM is remineralized, most of the fixed Cd (and PO_4^{3-}) is released back to seawater, leading to marine Cd distributions that resemble those of the major algal nutrients (e.g., Bruland, 1980). The physiological mechanisms underpinning the similarities between dissolved Cd and PO_4^{3-} concentrations are controversial, however. Several possible explanations have been put forward, ranging from true biochemical utilization of Cd by diatoms in a cambialistic Cd/Zn carbonic anhydrase (Lane et al., 2005), to mistaken uptake followed by internal storage and detoxification (Horner et al., 2013). Nonetheless, the remarkable similarity of Cd distributions to the other marine macronutrients has proven particularly valuable in Quaternary paleoceanography, and has enabled the successful reconstruction of water mass PO_4^{3-} concentrations from the Cd/Ca ratios of foraminiferal tests (e.g., Boyle, 1988; Marchitto and Broecker, 2006), and of paleoproductivity from the Cd concentration of clastic sediments (e.g., Brumsack, 2006; Wagner et al., 2013).

More recently, improvements in seawater sampling techniques and isotopic analytical capabilities have revealed large and systematic variations in the Cd-isotopic composition of seawater. These variations are thought to reflect the preferential uptake of isotopically light Cd by phytoplankton (Lacan et al., 2006; John and Conway, 2014), which renders residual Cd-depleted surface waters isotopically heavy by up to several permil (e.g., Ripperger et al., 2007; Abouchami et al., 2011, 2014; Xue et al., 2012, 2013; Conway et al., 2013). Studies of Cd-isotopic fractionation in seawater demonstrate that dissolved Cd-isotopic compositions are strongly related to the extent of Cd (and by association, PO_4^{3-}) utilization in surface waters, modulated by ocean circulation (e.g., Abouchami et al., 2011; Xue et al., 2013). As such, the Cd-isotopic composition of surface seawater and corresponding exported organic products offer an independent measure of macronutrient use efficiency in the upper ocean. The release of Cd by degraded sinking phytoplankton in deeper waters, and the long residence time of Cd in the oceans (~50 kyr; Morford and Emerson, 1999), means that water masses below ~200–500 m exhibit largely homogeneous Cd-isotopic compositions that are significantly lighter than the overlying surface waters (e.g., Ripperger et al., 2007). Because of this, the upwelling source of Cd to the surface ocean – the dominant source of Cd to surface-dwelling marine phytoplankton (e.g., Martin and Thomas, 1994) – is largely isotopically homogeneous throughout much of the oceans. These investigations of Cd-isotopic fractionation in the modern ocean thus enable the application of Cd-isotopic measurements to geological samples as a tracers of macronutrient utilization efficiency in past surface ocean environments.

Organic-rich shales are a particularly good candidate for reconstructing the efficiency of nutrient utilization from Cd-isotopic measurements. Although Cd has only a single oxidation state of +2, sedimentary Cd enrichments are primarily controlled by the redox state of oceanic bottom waters and sedimentary porewaters via two mechanisms. Firstly, the preservation of sinking OM, and the Cd contained therein, is greatly improved in anoxic waters/sediments compared to oxic settings. Secondly, anoxic conditions favor the co-precipitation of labile Cd with sulfides that form in the sediment (e.g., Framson and Leckie, 1978), and possibly even the water column itself (Janssen et al., 2014); Cd adsorption to OM may also be facilitated. Consequently, sedimentary Cd enrichments patterns in shales from modern continental margins closely follow those of redox-sensitive elements with multiple oxidation states (e.g., Mo, U and Re; Morford and Emerson, 1999; Nameroff et al., 2002). Although potential Cd-isotopic fractionation related to Cd precipitation in shales and/or sulfides is not well understood, indirect evidence suggests that CdS may be isotopically lighter than ambient seawater (e.g., Schmitt et al., 2009; Janssen et al., 2014). Despite this uncertainty, our data suggest that the Cd-isotopic composition of organic-rich sediments ultimately reflects the Cd-isotopic signature of OM in surface waters. This may come about either directly from organically-bound Cd within the sediment, or indirectly from remineralized OM-bound Cd that coprecipitates into sulfides in bottom/pore waters. Regardless, sedimentary Cd-isotopic compositions ultimately depend on the Cd-isotopic composition of the sinking particulate OM that is exported from the surface to the sediment.

Here, we apply Cd-isotopic measurements to reconstruct macronutrient utilization efficiency in a past marine environment, using modern ocean Cd-isotopic systematics as our interpretive framework. We focus on a series of organic-rich shales from Greenland and offshore Norway that were deposited during the onset of ocean anoxia prior to the latest Permian mass extinction. Sedimentary N-isotopic compositions (nitrogen) and trace metal geochemistry are used to reconstruct the quantity of upwelled nutrients (supply), and Cd-isotopic compositions are used to interpret the degree of macronutrient utilization (demand). Thus, these data enable the reconstruction of past nutrient supply *and* demand (hence productivity), allowing us to single out the major cause – stagnation or upwelling – for the Late Permian anoxia in the Greenland–Norway basin.

2. Geological setting and sample selection

2.1. Geological context

Our study focuses on Upper Permian laminated shales of the Ravnefjeld Formation in East Greenland (GRL) (Surlyk et al., 1986; Piasecki and Stemmerik, 1991) and correlative intervals from the Lower Turbidite Unit in the mid-Norwegian shelf (MNS) (Bugge et al., 2002). These samples were deposited on the facing sides of a major extensional basin that developed between Greenland and Norway from the Middle Permian onwards (Surlyk et al., 1986; Bugge et al., 2002; Torsvik et al., 2002) at paleolatitudes of ~30°N. This basin was part of an elongated seaway that may have connected the Panthalassa Ocean with the Tethys Ocean, providing a pathway for interhemispheric water exchange (Sengör and Atayman, 2009).

The organic-rich intervals in GRL and MNS were deposited in anoxic bottom waters with interlayered bioturbated siltstones and sandstones likely representing periods of more oxic bottom water conditions. The two shelf sections (GRL and MNS) were deposited in fairly shallow water (Bugge et al., 2002). Detailed estimates for water depths during deposition of the Ravnefjeld Formation vary from 25 m up to 125 m in the different parts of the GRL Permian

basin (Surlyk et al., 1986). The shelf setting and overall similarity to the GRL section imply that MNS shales were also deposited in typical modern-day shelf water depths of <150 m (e.g., Pinet, 2011).

In GRL, the bulk of the Ravnefjeld Formation overlies the Wuchiapingian (e.g., Stemmerik et al., 2001; Wignall and Twitchett, 2002b) and possibly Lower Changhsingian (Henderson and Mei, 2000) carbonate mounds of the Wegener Halvø Formation, suggesting a younger, Late Wuchiapingian to Changhsingian age for the Ravnefjeld Formation. Biostratigraphic constraints for the age of the Lower Turbidite Unit in MNS are limited; this unit is considered Upper Permian based on correlation with the Ravnefjeld Formation in GRL (Bugge et al., 2002). Late Changhsingian (253–252 Ma) Re–Os ages for Upper Permian organic-rich intervals from GRL and MNS show that both shales were deposited just prior to the Late Permian mass extinction (Georgiev et al., 2011).

2.2. Materials

We focused on twelve drill core shale samples that were previously characterized for their Re- and Os-isotopic composition, total organic carbon (TOC) contents, and major and trace elements (Georgiev et al., 2011). Of these, nine were analyzed for Rock–Eval parameters to characterize maximum burial temperatures and the quality of preserved OM (Georgiev et al., 2012). Three organic-rich samples from the Triaselv area in GRL are from the Lower Laminated Unit of the Ravnefjeld Formation (GRL-LL, ~10 m core depth), accessed from drillcore GGU 303102 (Piasecki and Stemmerik, 1991; coordinates 71°31′19.71″N and 24°11′35.22″W). We analyzed nine MNS shale samples from drillcore IKU 6611/U-09-01 (Bugge et al., 2002; coordinates 66°20′24.89″N and 11°48′46.59″W). Of these, three were from the Bottom Shale (MNS-BS, ~279 m core depth); three from the Lower Laminated Unit (MNS-LL, ~255 m core depth), and three from the Upper Laminated Unit (MNS-UL, ~241–244 m core depth). Additional details on sampling locations and preparation of sample powders are given in Georgiev et al. (2011, 2012).

3. Methods

We used separate powder aliquots of previously prepared drillcore powders (Georgiev et al., 2011, 2012) for Cd- and N-isotopic analyses and supporting geochemical measurements, including determination of TOC, major and trace element concentrations, pyrite framboid analyses, and Rock–Eval characterization of OM. A methodological overview is provided below; additional details are reported in the SI (Supplementary Information).

3.1. Partial shale digestions for Cd work

We employed inverse *aqua regia* (iAR, 1 part conc. HCl: 3 parts conc. HNO_3) for partial shale digestion, as this preferentially dissolves authigenic shale components (e.g., organic compounds, pyrite, carbonate) and leaves most detrital minerals (e.g., quartz, phyllosilicates, feldspar) intact (Selby and Creaser, 2003; Xu et al., 2012). Selective leaching of the authigenic shale components minimizes potentially significant uncertainties in the interpretation of Cd-isotopic results, namely the amount and Cd-isotopic composition of detrital material, enabling comparison of samples with variable detrital contributions. All twelve samples were digested in iAR; the supernatant was used for Cd-isotopic analyses, while the dried solid residue was weighed to calculate the fraction of shale digested by the iAR. Two total analytical blanks were prepared by mirroring all sample iAR-digestion steps. Partial digestion using CrO_3–H_2SO_4 proved unsatisfactory because of higher Cd blanks and lower Cd yields (see SI).

3.2. Cd-isotopic measurements

An appropriate amount of ^{111}Cd–^{113}Cd double spike was added to each sample and allowed to equilibrate at 120 °C. Cadmium was purified by passing the spiked samples through a two-stage ion-exchange chromatographic separation, as described in Wombacher et al. (2003).

Cadmium stable isotopic compositions were measured on a Nu Instruments Nu Plasma multi-collector HR-ICP-MS at the University of Oxford. An Elemental Scientific PFA MicroFlow Nebulizer was used for sample introduction in conjunction with a Nu Instruments DSN-100 desolvation system. Ion currents from 110 AMU (atomic mass unit; ^{110}Cd, ^{110}Pd) to 117 AMU (^{117}Sn) were simultaneously determined in 40 × 10 s integrations. Double spike data reduction, including spectral interference corrections, was performed offline using a MATLAB-based script. Cadmium-isotopic compositions are reported in the δ-notation relative to NIST SRM 3108 (Abouchami et al., 2012), with $\delta^{114/110}Cd_{NIST} = ([^{114/110}Cd_{sample}/^{114/110}Cd_{NIST}] - 1) \times 1000$.

Uncertainties are reported at the 2SD level, and depend mostly on the Cd content of the sample in question, ranging from $\delta^{114/110}Cd \pm 0.05‰$ up to $\pm 0.09‰$ (see SI). Analytical blanks for two separate iAR digestions yielded Cd contributions of 21 and 34 pg, respectively. Given such trace levels of Cd contamination – ranging between 0.01 and 0.08% of the total Cd present in any iAR-digested sample – we did not apply blank corrections to the Cd-isotopic and concentration data.

Detailed metal budget calculations for the samples show that almost all Cd liberated from the samples is non-lithogenic in origin (>98% for organic-rich shales; >89% for MNS-BS shale; see SI). As iAR digestion releases only a small portion of the lithogenic component, we estimate that detrital Cd contributes <0.3–1.4% of the iAR-released Cd for organic-rich rock and <8.7% for MNS-BS, and has only a negligible impact on the reported Cd-isotopic compositions. In addition, leaching tests conducted on modern continental margin sediments comparing iAR with 2 M HCl – whereby the latter was shown to leach only the authigenic Cd component (van Geen et al., 1995) – yielded identical Cd-isotopic compositions and Cd concentrations (see SI). This suggests that iAR leaching is an appropriate leach for the analysis of Cd-isotopic compositions of shales.

3.3. Rock–Eval pyrolysis

Rock–Eval parameters recorded during controlled pyrolysis of shale powder characterize the quality of preserved OM (Espitalié et al., 1980; Peters, 1986). New Rock–Eval data for MNS-BS shale were obtained at Statoil ASA Norway with a Rock–Eval 6 Turbo version 9.0 (1999) pyrolyser. Results for all other samples and associated methods are discussed in detail elsewhere (Georgiev et al., 2012).

3.4. Pyrite framboids

The morphology and size of individual pyrite crystals and framboidal (i.e. raspberry-shaped) aggregates in shale provide important paleoredox constraints (Wilkin et al., 1996). Eight polished thin sections were prepared from drill core pieces that are vertical equivalents of the facing shale piece consumed for powder preparation (four samples), from immediately adjacent vertical intervals (three samples), or from the stratigraphically nearest sample (one sample). The diameter of pyrite framboids was measured using a scanning electron microscope (SEM) operated in backscattered electron mode at 15 keV. All framboids visible on 500× images were measured individually with a measuring software at 3000× magnification.

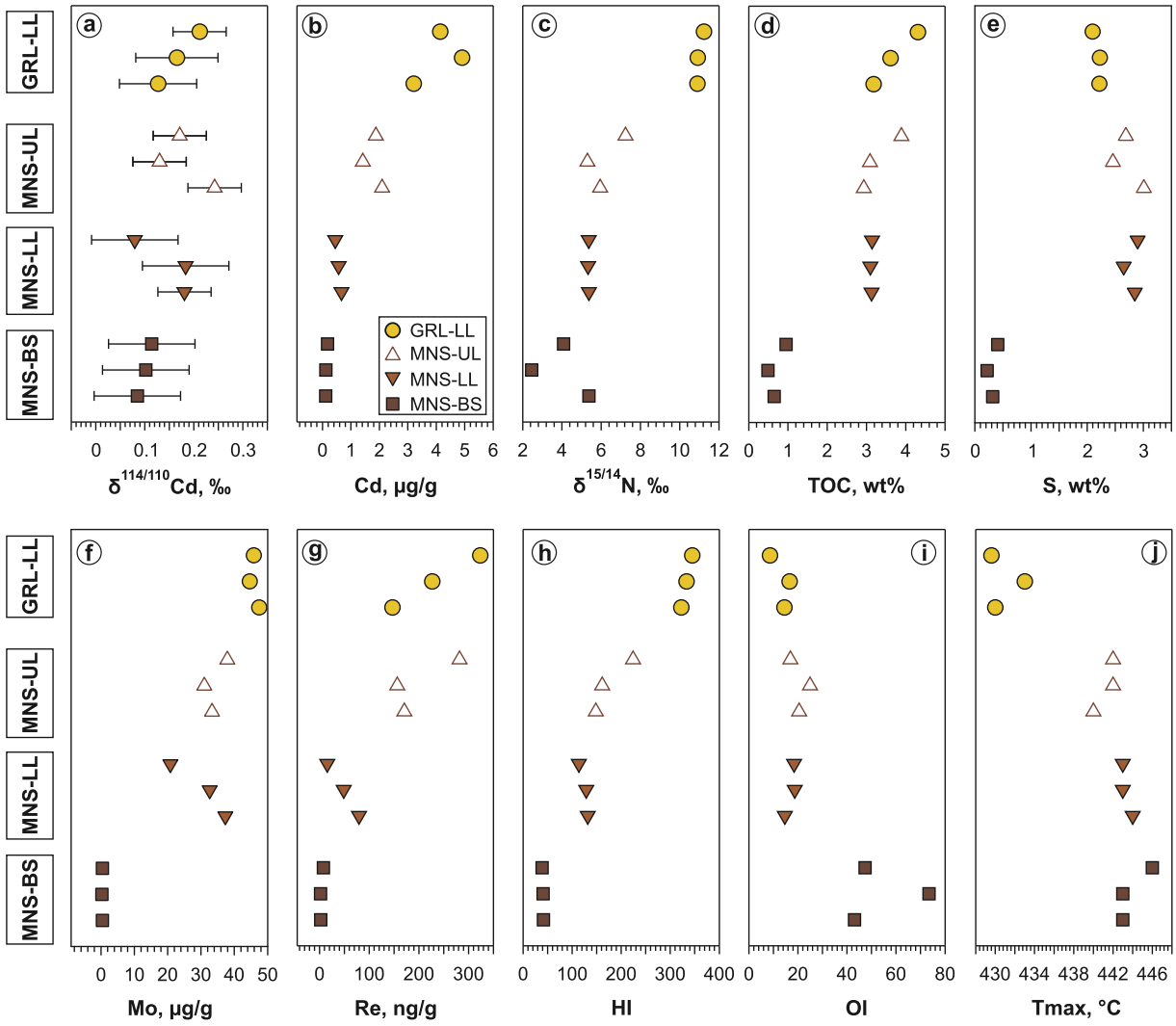

Fig. 1. Stratigraphic variations of Cd concentration and isotopic composition (a, b), N-isotope data (c), key major and trace element concentrations (c–g) and Rock–Eval parameters (h–j) in shales from East Greenland (GRL) and the mid-Norwegian shelf (MNS). Cd-isotopic compositions are expressed as $\delta^{114/110}$Cd values (in ‰) relative to NIST SRM 3108; N-isotopic compositions are expressed as $\delta^{14/15}$N (in ‰) relative to air. Hydrogen index (HI) is the amount of hydrocarbons generated through thermal cracking of nonvolatile organic matter, in units of mg hydrocarbons/g TOC. Oxygen index (OI) represents the amount of oxygen relative to the amount of organic carbon, expressed in units of mg CO_2/g TOC. Tmax is the temperature of maximum hydrocarbon generation during pyrolysis. Samples are vertically arranged in the correct relative stratigraphic order within each individual unit, or among the different MNS units, but note that the studied MNS intervals are separated by ~10–20 m thick unsampled intervals of bioturbated siltstones and sandstones (Bugge et al., 2002). The organic-rich GRL-LL is broadly correlative to the organic-rich MNS-LL and MNS-UL units (Bugge et al., 2002; Georgiev et al., 2011), but available data do not warrant finer stratigraphic correlations. For clarity, GRL data is plotted above the MNS data.

3.5. Major and trace elements

Whole-rock (WR) element abundances in eleven samples were determined to characterize shale compositions and estimate detrital Cd contributions. All analyses were obtained by Actlabs (Canada) using a uniform multi-acid digestion ($HF + HClO_4 + HCl + HNO_3$). Element concentrations were measured by ICP-AES or ICP-MS; both methods have a 1 SD reproducibility ±10%. Here, we report new WR data for three samples and employ these together with additional published WR data for eight samples and results for *aqua-regia* (AR) partial digestion for all twelve samples (Georgiev et al., 2011).

3.6. Nitrogen-isotopic analyses

Nitrogen concentrations and isotopic ratios in sediment powders were measured using an Europa Scientific 20–20 N-isotopic ratio mass spectrometer linked to an Europa Scientific RoboPrep-CN elemental analyzer, at Iso-Analytical, UK. Nitrogen isotopic ratios are reported using the standard δ-notation between the sample and air, where $\delta^{15/14}N_{air} = ([^{15/14}N_{sample}/^{15/14}N_{air}] - 1) \times 1000$. Analytical precision of $\delta^{15/14}$N estimated from multiple analyses of standards was ±0.22‰ (2 SD).

4. Results

Tabulated results are presented in the SI and summarized below.

4.1. Cd contents

Dry solid residues following inverse *aqua regia* (iAR) acid digestion had between 73 and 84 wt% of the original powder mass (92 wt% for sample ORG-388; SI), indicating that iAR dissolved from 16 to 27 wt% of the shale (8 wt% for sample ORG-388). Cadmium in shales dissolved with iAR varies from 0.12 µg/g to 4.91 µg/g, with notable variations between the four studied groups (stratigraphic intervals) of samples (Fig. 1). In MNS-BS, relatively low Cd contents of 0.12 to 0.18 µg/g are similar to or slightly

higher than average upper crustal rocks with 0.09–0.10 μg/g Cd (Rudnick and Gao, 2004; Wedepohl, 1995). Cadmium contents in the stratigraphically higher MNS-LL shales vary between 0.45 and 0.67 μg/g. These values are approximately four times higher than in MNS-BS, and higher than Cd estimates for the upper continental crust (see above) or for average shale (0.30 μg/g, Turekian and Wedepohl, 1961). The uppermost studied shales from MNS-UL have the highest Cd contents among MNS samples (1.41 to 2.10 μg/g); Cd concentrations of GRL-LL shales reach values of 3.21 to 4.91 μg/g.

4.2. Cd-isotopic composition

Following iAR digestion, the shales have $\delta^{114/110}$Cd of between +0.08 and +0.24‰, with a mean $\delta^{114/110}$Cd of $+0.15 \pm 0.01$‰ (2 SE, $n = 12$). The mean $\delta^{114/110}$Cd of all MNS samples ($+0.14 \pm 0.02$‰, 2 SE, $n = 9$) is equivalent to the mean value of all GRL samples ($+0.17 \pm 0.02$‰, 2 SE, $n = 3$). Within MNS samples, one-way non-paired ANOVA tests show the statistical equivalence at the 2 SD level ($p = 0.23$) of $\delta^{114/110}$Cd between the BS unit ($+0.10 \pm 0.01$, 2 SE, $n = 3$), the LL unit ($+0.15 \pm 0.03$, 2 SE, $n = 3$), and the UL unit ($+0.18 \pm 0.03$, 2 SE, $n = 3$). MNS-UL and MNS-BS samples show the largest difference in mean values (0.08‰), though this offset is not significant at the 2 SD level ($p = 0.08$). Thus, all 12 samples from the 4 samples groups at both localities (GRL and MNS) have statistically identical Cd-isotopic compositions. Overall, Cd-isotopic values of iAR-digested shales do not co-vary with major changes in [Cd] ($r = 0.50$, $p = 0.10$, $n = 12$), though if only the MNS samples are considered, the correlation between [Cd] and Cd-isotopic composition becomes statistically significant ($r = 0.73$, $p = 0.03$, $n = 9$).

4.3. WR geochemistry, Rock–Eval, nitrogen-isotopic data, and pyrite framboid analyses

The most characteristic geochemical features of the samples are the high TOC, [S], and trace metal content of laminated MNS-LL, MNS-UL and GRL-LL units compared to the bioturbated MNS-BS (Fig. 1). In addition, Cd and redox-sensitive metals (Mo, Re, Se, Tl, U) systematically increase from MNS-LL through MNS-UL to GRL-LL units. This is accompanied by a constant or even slightly decreasing sulfur and TOC abundances, and decreasing Al, P, and total Fe abundances in this direction (Georgiev et al., 2011).

Nitrogen-isotopic analyses show a clear stratigraphic trend towards more positive $\delta^{15/14}$N upsection in MNS, ranging from +2.46‰ in MNS-BS to +7.24‰ in MNS-UL; GRL-LL displays the heaviest $\delta^{15/14}$N of +10.90 to +11.23‰ (Fig. 1).

Rock–Eval parameters demonstrate the contrasting OM properties in the TOC- and sulfur-lean MNS-BS compared to all other TOC- and sulfur-rich units (Fig. 1). Low hydrogen indices (HI) and high oxygen indices (OI) in MNS-BS are typical of terrestrial and/or oxidized OM, whereas the higher HI and low OI of the organic-rich shales suggest mixed marine/terrestrial contribution and/or better preservation of the OM during shale deposition. The two studied sections have different thermal maturities, a measure for the maximum paleotemperatures reached upon burial of the shale. In MNS shale, T_{max} of ~442 °C corresponds to maximum paleotemperatures of ~80–90 °C, whereas a lower T_{max} of ~430 °C for GRL shales corresponds to ~50–60 °C maximum paleotemperatures (see Hunt, 1995, for discussion of maturity parameters).

SEM images (Fig. 2) and pyrite size analyses (Fig. 3a) show a clear distinction between MNS-BS and the remaining TOC-rich units. Pyrite, mostly in the form of framboids, but also as cubic crystals, is rarely observed in MNS-BS (Fig. 2a), whereas pyrite framboids are abundant in MNS-LL, MNS-UL and GRL-LL units (Figs. 2b–f). The average size of pyrite framboids in MNS-BS (6.2–6.5 μm) is larger than in the two overlying MNS units (3.8–4.1 μm) and in GRL shale (3.4–3.5 μm) (Fig. 2e–f; Fig. 3a).

5. Discussion

5.1. Redox conditions and metal sources

5.1.1. Redox conditions during shale deposition

The two studied shale sections (GRL and MNS) record primary geochemical signatures relating to deposition and early diagenesis (Georgiev et al., 2012; SI). Previous studies emphasize the lack of bioturbation, with abundant OM, sulfur, and redox-sensitive metals in the GRL-LL and in MNS-LL and MNS-UL units as evidence for shale deposition in oxygen-deficient waters (Piasecki and Stemmerik, 1991; Bugge et al., 2002; Georgiev et al., 2011). In contrast, the lower abundance of OM, sulfur, and redox-sensitive metals in MNS-BS argue for more oxygenated bottom-water conditions during deposition (Georgiev et al., 2011). Combining our new pyrite framboid, Rock–Eval, and trace element geochemical data, we assign the following redox environments: GRL-LL was deposited in euxinic bottom waters, whereas MNS-LL and MNS-UL were deposited in euxinic to anoxic bottom waters, and MNS-BS was deposited in bottom waters with only mild- to moderate oxygen restriction (Fig. 3). In the mid-Norwegian shelf, bottom water anoxia intensified approaching the end-Permian, from the bottom (MNS-BS), through the intermediate (MNS-LL), to the top studied interval (MNS-UL). This paleoredox information (outlined in detail in the SI) provides the framework for interpreting the sources and sinks of Cd and other metals in the shales.

5.1.2. Major sources of Cd and other metals: a sedimentary mass balance

The sedimentary Cd budget is largely controlled by authigenic Cd enrichments (or depletions) in addition to Cd contained within OM or detrital minerals; marine carbonates do not significantly contribute to Cd removal (Boyle, 1988) or Cd-isotopic fractionation in seawater (Horner et al., 2011). As each of these components may have a different Cd-isotopic signature, we first attempt to quantitatively constrain their proportions in the studied sediments before discussing their Cd-isotopic compositions. Details on the calculations are given in the SI and summarized below.

We calculate detrital contributions based on generalized shale mineralogy and knowledge of the weight of the residue following iAR digestion, assuming that detrital minerals supplied elements at typical upper crustal concentrations (Rudnick and Gao, 2004). For biologic contributions, using our TOC and Rock–Eval data we first calculate the proportion of different OM types present in shale (Cornford, 1998; Peters, 1986), and the amount of OM lost to hydrocarbon generation (formula of Cornford, 1998 and Cornford et al., 2001). We then sum these contributions to estimate the amount of biologically supplied carbon. The molar amount of Cd directly supplied to the sediment by OM is calculated by multiplying the organic carbon content by the extended (molar) Redfield Cd:C ratio of modern marine phytoplankton (Redfield, 1934; Cd data from Ho et al., 2003). Our calculations show that 1 wt% carbon (TOC) in sediments provides 0.16 μg biologic Cd per gram sediment. This value, which we recommend for calculating biologic Cd contributions to sediments, is ~5 × higher than previous estimates (e.g., Rosenthal et al., 1995). Authigenic Cd contributions were calculated as the difference between the measured concentration and the sum of the detrital and biological contributions (Fig. 4).

Our results show that for Cd, biologic contributions prevail in MNS-BS (66–88%) and MNS-LL (76–96%), and decrease in MNS-UL (26–43%) and GRL-LL (12–16%) intervals. Detrital Cd contributions

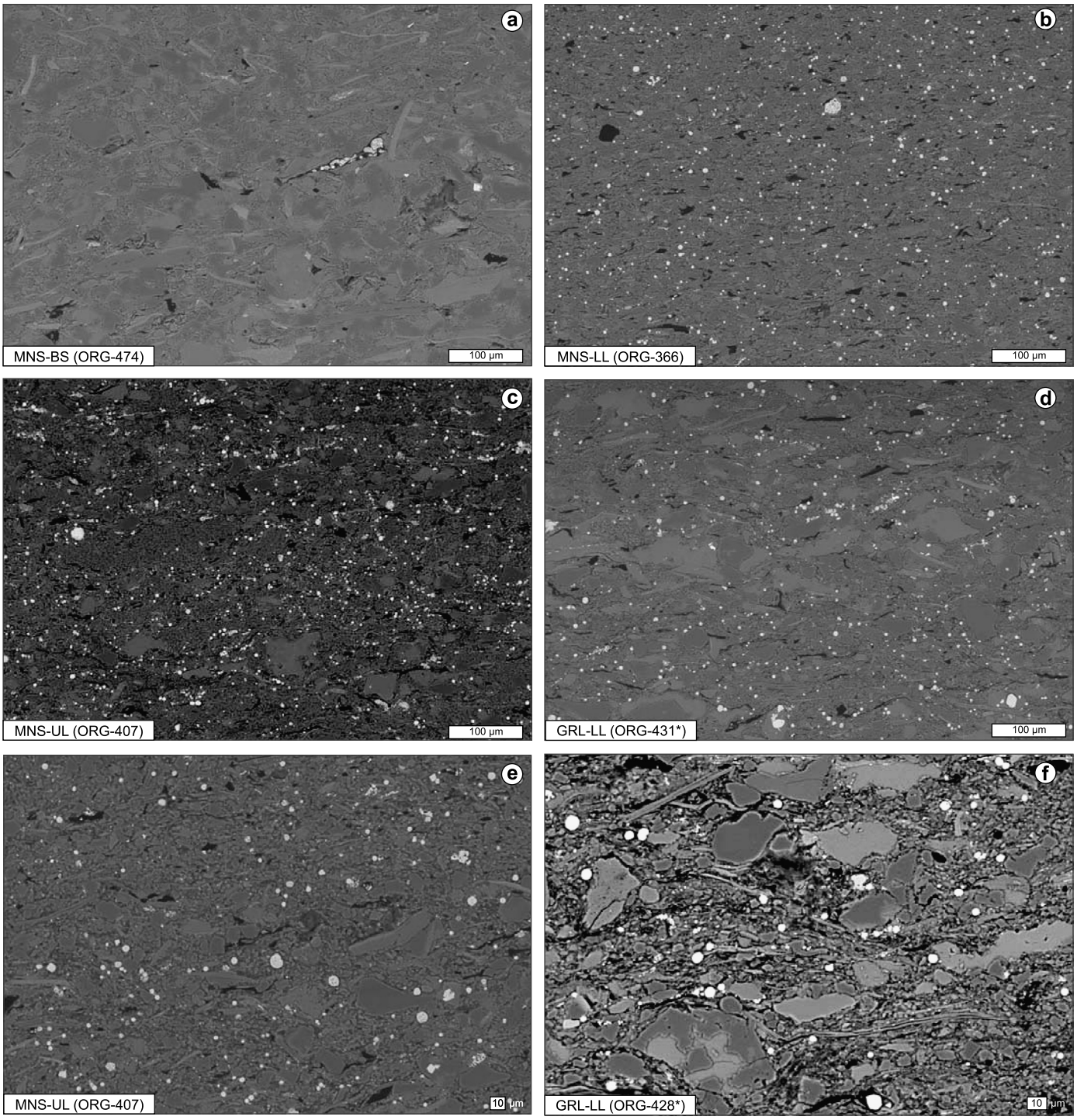

Fig. 2. SEM backscattered electron images of polished thin sections of shale. Spherical pyrite framboids appear as bright regions. Note the scarcity of pyrite in MNS-BS shale (panel a) as opposed to the abundance of framboids in MNS-LL, MNS-UL, and GRL-LL shale (panels b–d). Panels e–f are at greater magnification than panels a–d (see scale bar). Images from GRL-LL unit are taken from drillcore samples immediately adjacent to ORG-431 and ORG-428 (see SI).

are negligible in all organic-rich units (<1.5%), but are somewhat higher in MNS-BS (5–11%). Authigenic processes in MNS-BS and MNS-LL units result in relatively small Cd enrichments or depletions compared to the total Cd budget (average authigenic Cd fraction is 0.0 ± 0.2, 1SD, $n = 6$). In contrast, MNS-UL and GRL-LL units show significant authigenic enrichments: authigenic fractions contribute 57–73% and 84–88% of the total Cd, respectively.

The above-calculated fractions enable a more detailed interpretation of the Cd-isotopic composition of the shales. Further, detrital, biologic and authigenic fractions for P, Mo, and Re, calculated in a similar way as described for Cd, provide additional constraints on the paleoredox state of bottom waters during shale deposition, which all support independent evidence from other paleoredox proxies (see discussion in SI).

5.1.3. Sedimentary trace metal associations

Authigenic Cd enrichments in shales are thought to occur via the trapping of labile Cd in Cd sulfides or Fe–Cd sulfides in

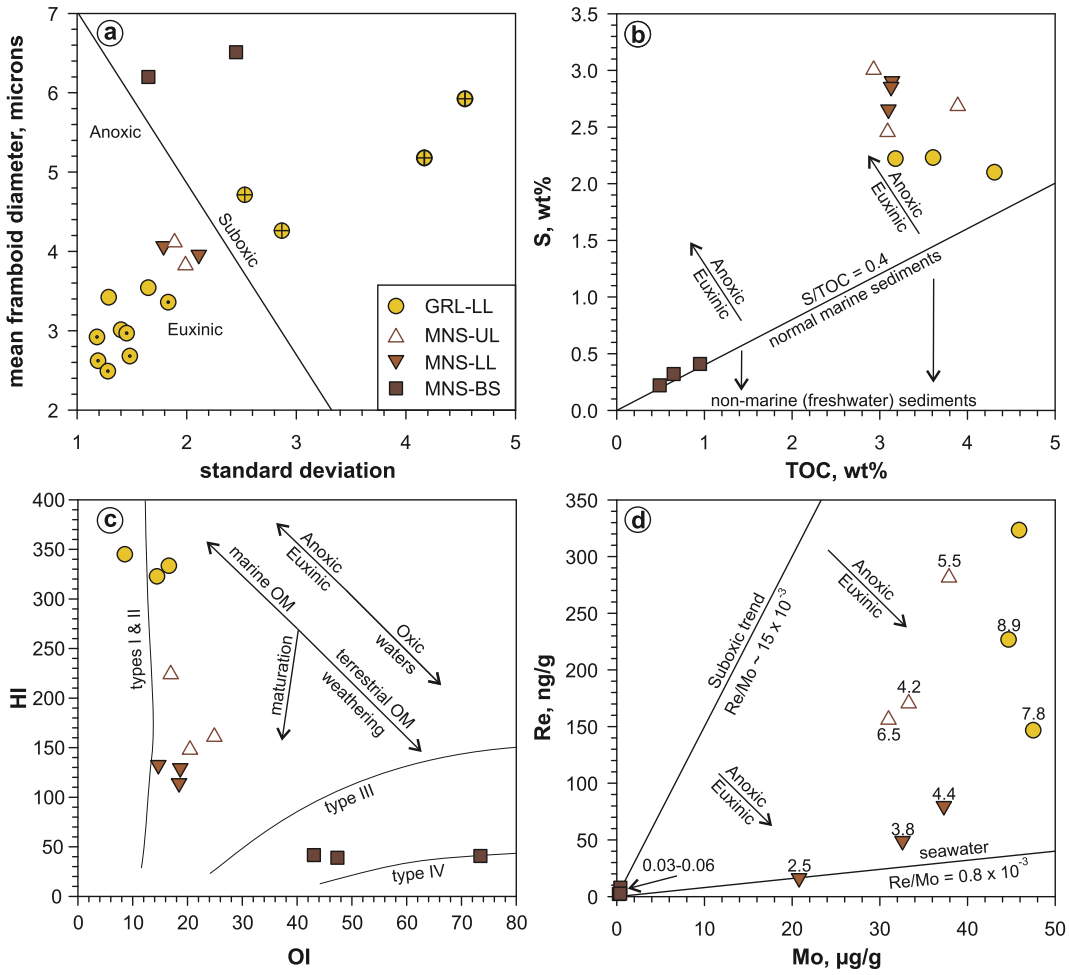

Fig. 3. Plots discriminating bottom water redox conditions during shale deposition. (a) Mean pyrite framboid size vs. standard deviation diagram. The boundary line separates modern-day euxinic/anoxic from suboxic bottom water environments (Wilkin et al., 1996). Additional data for the Ravnefjeld Formation in East Greenland (Nielsen and Shen, 2004) are shown with dotted circles (for laminated units) and crossed circles (for interlayered bioturbated units; (b) S vs. TOC content. Shales deposited below normally oxygenated bottom waters typically have S/TOC ratios near 0.4, whereas bottom water anoxia is usually reflected by S/TOC ratios in shale >0.5 (Berner and Raiswell, 1983); (c) Plot of hydrogen index (HI = 100∗S2/TOC, in units of mg HC/g TOC) versus oxygen index (OI = 100∗S3/TOC, in units of mg CO_2/g TOC), showing the contrasting properties of organic matter (OM) in MNS-BS shale. Arrows show the general effect of syn-depositional bottom water redox conditions, syn-depositional increasing proportions of terrestrial OM, and post-depositional oxidative weathering or thermal maturation, on the HI–OI relations in shale. Trends for the main OM types taken from Hunt (1995); (d) Re vs. Mo content in shale. High sedimentary Re/Mo ratios reflect deposition in suboxic bottom waters, whereas lower Re/Mo ratios approaching that of seawater reflect deposition in anoxic/sulfidic bottom (Crusius et al., 1996). Suboxic Re/Mo value and trend taken from Böning et al. (2004) and Turgeon and Brumsack (2006). Numbers adjacent to samples show an additional paleoredox proxy – the Mo/Al weight ratios in sediments (multiplied by 10^4).

reducing sediments (e.g., Framson and Leckie, 1978; Rosenthal et al., 1995; van Geen et al., 1995; Parnell et al., 2014). That authigenic Cd enrichments generally start early in the diagenetic cycle before the onset of sulfate – or even iron reduction (Rosenthal et al., 1995; Morford and Emerson, 1999), is explained by the presence of microsulfidic environments within the sediment (Rosenthal et al., 1995), with labile Cd sourced from respiration of sedimentary OM (McCorkle and Klinkhammer, 1991). Pyrite is by far the most abundant sulfide in the studied shales (Fig. 2; see also Nielsen and Shen, 2004), and syngenetic and diagenetic sedimentary pyrite may be highly enriched in trace metals (Huerta-Diaz and Morse, 1992; Large et al., 2014).

However, in the organic-rich samples from this study, total (and authigenic) Cd correlates negatively with sulfur content, and positively with TOC, particularly with types I and III TOC (SI), suggesting that Cd is largely associated with sedimentary OM (Fig. 1; SI). Other studies have identified similar metal-OM associations in other organic-rich shales (e.g., Chappaz et al., 2014), even for elements, such as Mo, that are only authigenically enriched in the presence of sulfidic (pore)waters (Crusius et al., 1996; Helz et al., 1996).

5.2. Sedimentary Cd-isotopic analyses as a proxy for marine nutrient utilization

The application of Cd-isotopic data for shales to reconstruct aspects of the Late Permian environment requires understanding the Cd and Cd-isotopic cycle in the modern oceans. Phytoplankton preferentially assimilate isotopically light Cd from seawater (e.g., Lacan et al., 2006), driving residual Cd-depleted surface waters towards more positive $\delta^{114/110}$Cd values as high as +3 to +4‰ (Ripperger et al., 2007). The relatively constant Cd-isotopic composition of intermediate and deep waters of $\delta^{114/110}\text{Cd} = +0.3 \pm 0.03$‰ (2 SE, $n = 27$) at variable Cd contents of 0.4 to 1.0 nM (Ripperger et al., 2007; Xue et al., 2013) implies that particulate OM, which sinks to these depths and supplies dissolved Cd by remineralization, is also characterized by a relatively constant $\delta^{114/110}$Cd of +0.3‰. This pattern persists because biological Cd removal from much of the surface ocean is essentially quantitative (Ripperger et al., 2007). However, in regions of incomplete nutrient uptake, such as the high nutrient low chlorophyll zone of the modern Southern Ocean, or regions with significant upwelling, exported biological material is characterized by

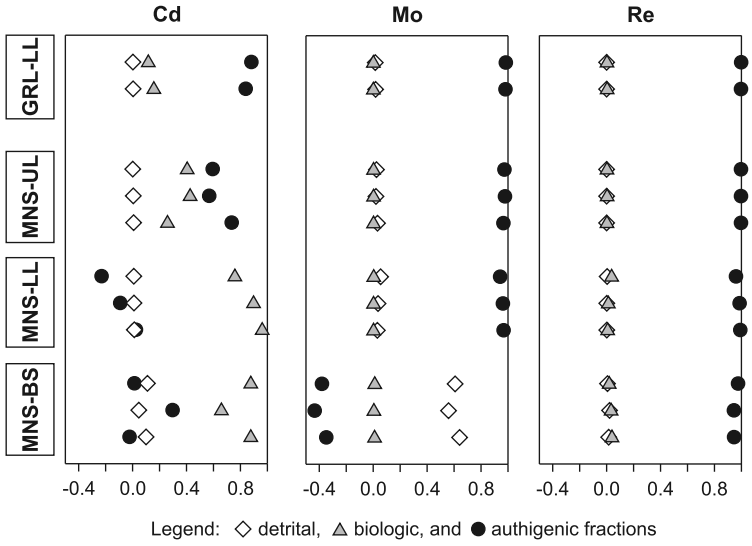

Fig. 4. Relative proportions of authigenic (circles), biologic (triangles), and detrital contributions (diamonds) in the studied samples, expressed as fractions. Biologic contributions were calculated based on measured TOC + TOC lost to hydrocarbon generation. The absolute values of the three calculated fractions for each element and sample must sum to unity. The 'authigenic' contribution is used to balance the residual [Me], such that negative and positive authigenic fractions indicate authigenic depletions and enrichments, respectively. See text and SI for additional details.

Cd-isotopic compositions that are up to ~0.4‰ lighter relative to the source of dissolved Cd from upwelling (+0.3‰; e.g., Xue et al., 2013). Thus, Cd-isotopic data for OM in marine sediments should have $\delta^{114/110}$Cd values between about −0.1 (little utilization) to +0.3‰ (complete utilization), that scales with the degree of surface water Cd utilization – and more generally, 'nutrient' utilization.

Using these systematics, we envision three general scenarios for the interpretation of Cd content and Cd-isotopic data in organic-rich sediments (Fig. 5): (A) low nutrients – complete consumption, (B) high nutrients – complete consumption, and (C) high nutrients – incomplete consumption (panels A, B, and C, respectively). In scenarios (A) and (B) nutrient utilization will be nearly complete such that the Cd-isotopic composition of exported OM will resemble the upwelling source (i.e. $\delta^{114/110}Cd_{OM} \approx +0.3‰$). However, productivity is unconstrained by $\delta^{114/110}Cd_{OM}$, as the total amount of OM production is dependent on the nutrient supply to the euphotic zone. If the upwelling supply of nutrients is low (Fig. 5A; e.g., stratified basin), productivity will be low, and the Cd content of exported OM in underlying sediments will also be low, reflecting the restricted resupply of dissolved nutrients to the surface. Thus, shales from stratified basins tend to develop low metal/TOC ratios (e.g., Algeo and Lyons, 2006). When the resupply of nutrients is rapid (Fig. 5B; e.g., vigorous upwelling) and productivity is also high, the Cd content of OM in sediments will generally be higher. Therefore, the differences in sedimentary [Cd] and Cd/TOC ratios primarily reflect the amount of productivity when Cd utilization is near-compete (i.e. $\delta^{114/110}Cd_{OM} \approx +0.3‰$). In scenario (C), the upwelling supply of nutrients exceeds biological demand (Fig. 5C). Productivity is high – reflected in sedimentary OM with high [Cd] – but supply is even higher. Thus, surface water nutrient utilization will be incomplete, leading to OM with Cd-isotopic compositions that are lighter than the upwelling source, falling on a continuum between $\delta^{114/110}Cd_{OM} \approx -0.1‰$ and +0.3‰ that scales with the degree of nutrient utilization.

However, if nutrient reconstructions based on Cd-isotopic analyses of marine sediments are to be meaningful, it is important to understand how different Cd-containing phases and post-depositional processes may affect the Cd-isotopic composition of shales. The effect of diagenesis on the Cd-isotopic composition of shales has not been studied. Although we cannot rule out possible diagenetic effects on our $\delta^{114/110}$Cd data, several observations argue that the primary elemental concentrations and isotopic ratios of the samples remain, even after late diagenesis and burial. These include: (i) the preservation of pristine Re–Os isotopic systematics (Georgiev et al., 2012, see also SI); (ii) distinct and systematic variations in the isotopic composition of sedimentary nitrogen (Fig. 1c), trace metal concentrations, and Rock–Eval parameters (Fig. 1f–j); and (iii) the relatively low maximum paleoburial temperatures of 50–90 °C (Georgiev et al., 2012; this study). Further, precipitation of insoluble CdS – one of the several likely host phases for Cd in shales – rapidly and efficiently sequesters pore water Cd (e.g., Gobeil et al., 1987; Pedersen et al., 1989; Rosenthal et al., 1995, but see Sundby et al., 2004). This near-quantitative Cd removal (e.g., Elderfield et al., 1981) minimizes potential isotopic fractionation. Once formed, CdS is extremely stable under oxygen-poor sedimentary conditions ($K_{sp} = 10^{-27.8}$; e.g., Elderfield et al., 1981; Gobeil et al., 1997), therefore exchange of Cd with anoxic pore fluids during early diagenesis is unlikely.

Below, we briefly explore the Cd content and isotopic systematics of the three fractions that contribute Cd to shales (biologic, authigenic and detrital) and how this may affect interpretation of the aforementioned scenarios. Detrital contributions exert a negligible influence on the Cd-isotopic compositions compared to biologic and authigenic contributions, which have similar values, reflecting their common Cd source of remineralized OM.

5.2.1. The detrital fraction

Detrital input has a likely $\delta^{114/110}$Cd of ~0.0 ± 0.05‰ (average loess samples; Schmitt et al., 2009; Rehkämper et al., 2011). Detrital fractions, however, are small to negligible in all studied Upper Permian shales (Fig. 4, SI) and thus are not discussed further.

5.2.2. The biological fraction

The Cd-isotopic compositions of samples with predominantly biologically-sourced Cd (MNS-BS and MNS-LL; Fig. 4) indicates primary biological contributions from exported OM were characterized by $\delta^{114/110}Cd = +0.12‰$. These values are resolvably lighter than modern day seawater $\delta^{114/110}$Cd of +0.30‰ (Ripperger et al., 2007; Xue et al., 2013), which can be explained by two scenarios. If Late Permian seawater had a notably lighter Cd-isotopic composition than the modern ocean, quantitative Cd utilization could have resulted in OM characterized by $\delta^{114/110}Cd \approx +0.12‰$. Alternatively, Late Permian seawater had a Cd-isotopic composition

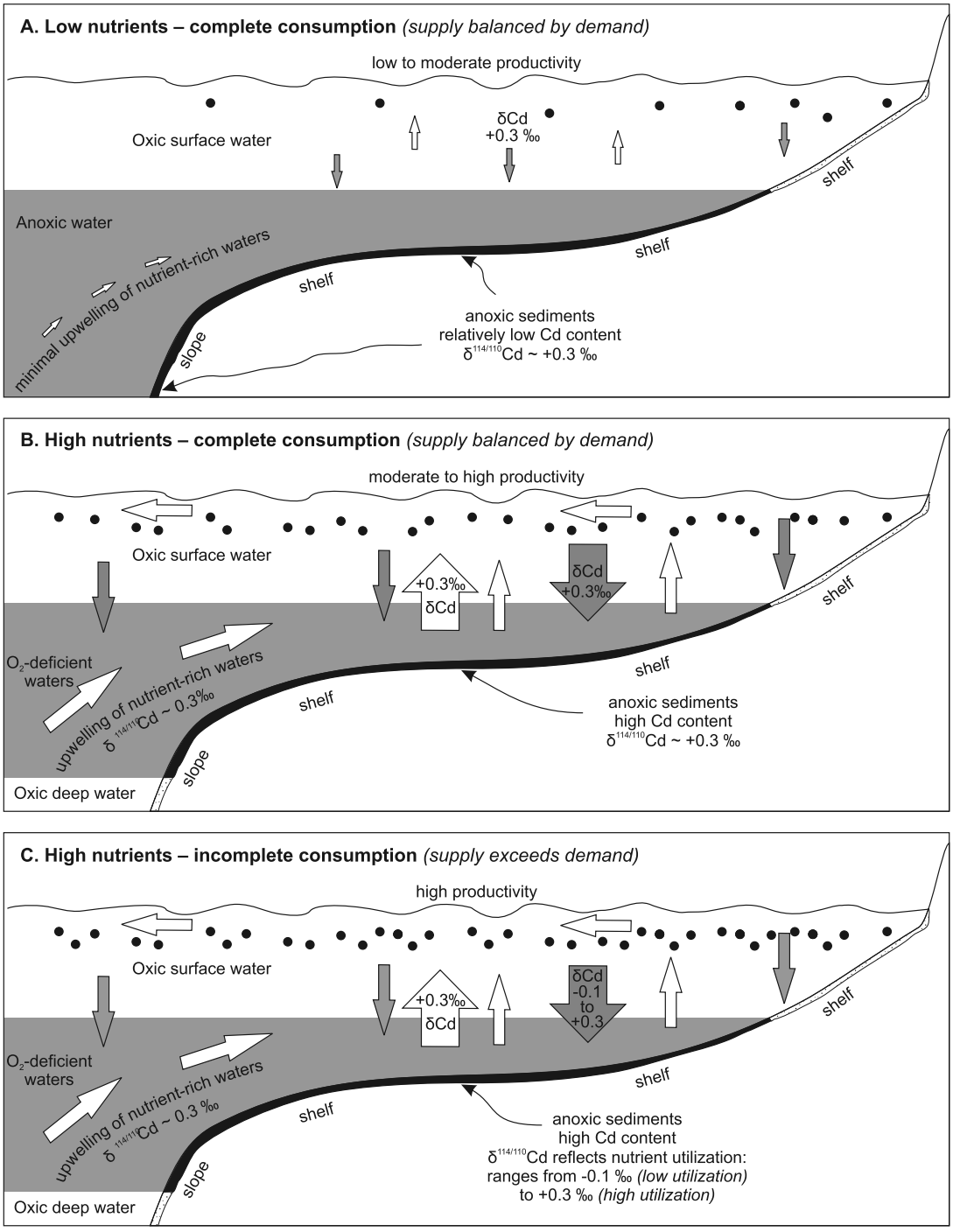

Fig. 5. Schematic cartoon illustrating three hypothetical scenarios for interpretation of Cd-isotopic data in organic-rich shales. (A) Low nutrients – complete consumption. Stagnant ocean with limited nutrient supply, where despite favorable preservation, sediments have relatively low Cd contents that reflect low productivity. Cd-isotopic compositions are primarily controlled by quantitative Cd uptake by phytoplankton, with $\delta^{114/110}$Cd reflecting quantitative nutrient drawdown. (B) High nutrients – complete consumption and (C) high nutrients – incomplete consumption. Upwelling deep waters provide ample nutrients to surface phytoplankton. The Cd content of organic-rich shales is variable depending on overall productivity, with $\delta^{114/110}$Cd depending on nutrient utilization efficiency. When uptake of dissolved Cd by phytoplankton is near-quantitative (high utilization efficiency), shale $\delta^{114/110}$Cd will approach the value of the upwelling deep water source (~0.3‰, panel B). However, when utilization efficiency is lower, $\delta^{114/110}$Cd is lighter and reflects the degree of nutrient utilization, scaling between nearly +0.3‰ (high nutrient utilization efficiency) to about −0.1‰ (low nutrient utilization; panel C). See main text for discussion.

similar to the modern value (+0.30‰), but the exported OM was characterized by isotopically lighter Cd due to incomplete biological utilization of Cd in surface waters. While there are currently no constraints on the Cd-isotopic composition of Late Permian seawater, this is of secondary significance as the constancy of the shale $\delta^{114/110}$Cd values up-section implies invariant levels of nutrient utilization through time, regardless of the Cd-isotopic composition of Late Permian seawater.

5.2.3. The authigenic fraction

The similar Cd-isotopic composition of shales with different biological and authigenic contributions shows that the authigenic

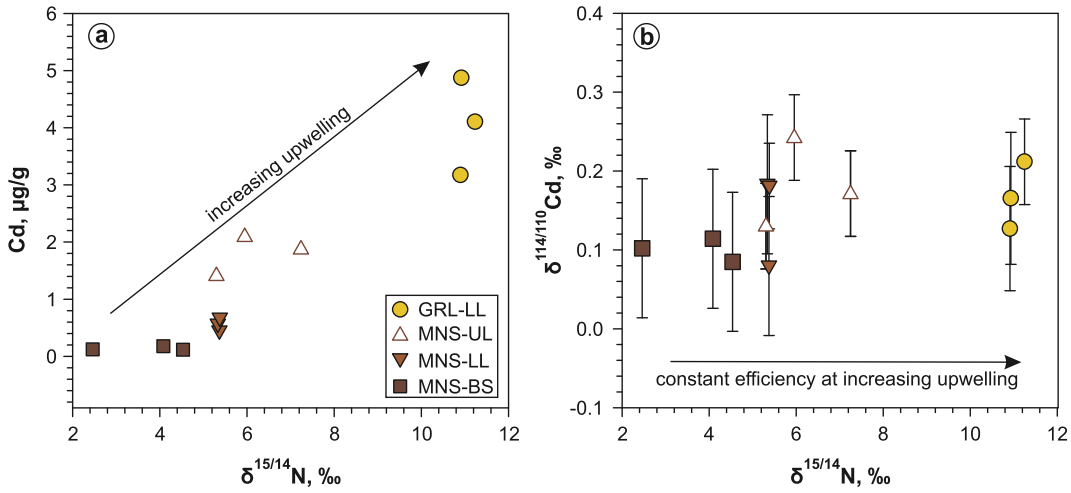

Fig. 6. (a) Cd content following inverse *aqua regia* digestion and (b) Cd-isotopic composition plotted against sedimentary $\delta^{15/14}$N. Positively correlated [Cd] (and Cd/Al, data not shown) and $\delta^{15/14}$N up-section indicate increasing nutrient supply from upwelling, whereas constant $\delta^{114/110}$Cd indicates invariant nutrient utilization. Increased paleoproductivity is thus required to maintain constant nutrient utilization when nutrient supplies are larger (e.g, from more intense upwelling).

fraction also possesses isotopically lighter Cd compared to modern deep seawater. In samples where authigenic Cd dominates (MNS-UL and GRL-LL; Fig. 4), $\delta^{114/110}\text{Cd} = +0.17 \pm 0.02‰$. Authigenic Cd is provided by three major mechanisms, all linked to the degradation of OM: (1) oxidation of OM in the oxic top portion of sediments (McCorkle and Klinkhammer, 1991; Rosenthal et al., 1995); (2) anaerobic decomposition of OM within the deeper, anoxic section of sediments; or (3) formation of insoluble CdS in the water column associated with OM remineralization (e.g., Janssen et al., 2014). In all scenarios, as Cd is released to ambient sea- or pore-water, it is rapidly reprecipitated in secondary minerals – likely CdS – that are remobilized when oxygen is present (e.g., Rosenthal et al., 1995), but stable under reducing conditions. While it is ultimately difficult to constrain the proportions of these specific delivery mechanisms, all three pathways are strongly related to the export and regeneration of OM from the euphotic zone, irrespective of the dominant bottom water conditions (e.g., oxic, 'suboxic', or anoxic ± sulfidic).

The studied shales were deposited under different bottom water redox conditions (Fig. 3). Suboxic waters partly favored oxic degradation of OM within the MNS-BS sediments, whereas anoxic and sulfidic bottom waters would have favored authigenic Cd preservation (e.g., Rosenthal et al., 1995) in the MNS-LL, MNS-UL and GRL-LL sediments. In GRL-LL, authigenic enrichments reach ~88% of the total Cd (Fig. 4), or ~4.3 µg/g Cd for sample ORG-431. If all this authigenic Cd was sourced from OM remineralized within the sediment, the sediment must have originally contained an additional 27 wt% TOC (or ~58 wt% OM), which was entirely decomposed to provide the needed authigenic Cd. Anoxic bottom water conditions at GRL-LL would have favored anaerobic OM decomposition within the sediments. Even though anaerobic degradation of OM could be very efficient (e.g., Jorgensen, 1982), the requirement for complete anaerobic decomposition of such high initial TOC seems unrealistic. Instead, the large authigenic enrichment likely points towards an additional Cd source in GRL-LL, possibly from CdS formation in the water column (e.g., Janssen et al., 2014), or direct CdS precipitation from anoxic bottom waters (e.g., Rosenthal et al., 1995). Rhenium and Mo – metals that are not dominated by microbial cycling and therefore likely sourced directly from seawater – also show significant authigenic enrichments in GRL-LL (Fig. 4). Since authigenic Cd enrichments closely follow enrichments of other redox-sensitive metals (e.g., Rosenthal et al., 1995), we conclude that some of the observed authigenic Cd fraction was also sourced directly from seawater. However, assessing the relative contribution of Cd sourced directly from anoxic bottom water compared with water column OM remineralization-associated CdS in GRL-LL is not currently possible. Regardless, the overall Cd-isotopic similarity of GRL-LL to all other samples indicates that the biological fraction of in GRL-LL is also characterized by $\delta^{114/110}\text{Cd} \approx +0.15‰$, indicative of incomplete nutrient utilization at the time of deposition.

5.3. Reconstructing nutrient utilization and primary productivity in the Late Permian

The redox, trace element, and Cd-isotopic data for the studied shales hone several paleoenvironmental assumptions about the Late Permian. The constant $\delta^{114/110}$Cd up-section implies the fraction of utilized nutrients remained constant during sediment deposition, regardless of the Cd-isotopic composition of the Late Permian ocean. Temporally-constant $\delta^{114/110}$Cd requires no quantitative drawdowns of Cd caused by increased productivity and/or interruption to the upwelling supply of nutrients. Substantial up-section increases of total [Cd] at both MNS and GRL sections suggests that more OM was exported to the sediments, either because of an increased nutrient supply or because of greater OM preservation (the latter requiring more anoxic bottom waters). When recast from a paleoredox perspective, these two possibilities parallel the two primary driving mechanisms that were able to sustain the Late Permian anoxia and contribute towards the subsequent mass extinction (e.g., Algeo et al., 2010; Isozaki, 1997). Put simply, was water-column anoxia developed and subsequently sustained by increased upwelling and productivity, or was increasing water-column anoxia caused by global warming and tectonic reconfiguration that cut off deep-water circulation?

The sedimentary N-isotopic data allow the discrimination of these hypotheses, requiring a relatively high degree of upwelling at both localities (Fig. 6). The $\delta^{15/14}\text{N–NO}_3$ (N-isotopic composition of dissolved nitrate) is relatively uniform in the oceans, presently at $\approx +5‰$, but was generally lower (-2 to $+2‰$) in warmer geologic periods, like the Jurassic or Cretaceous (Jenkyns et al., 2001). Regardless of the absolute background $\delta^{15/14}\text{N–NO}_3$, water-column denitrification in the nutrient-rich and oxygen-deficient continental margin upwelling zones drives $\delta^{15/14}\text{N–NO}_3$ toward substantially higher values (e.g., Algeo et al., 2008a). Settling and preservation of biomass that utilized this isotopically heavy nitrate results in high sedimentary $\delta^{15/14}$N, indicative of intense upwelling during sediment deposition (e.g., Quan et al., 2013). In contrast,

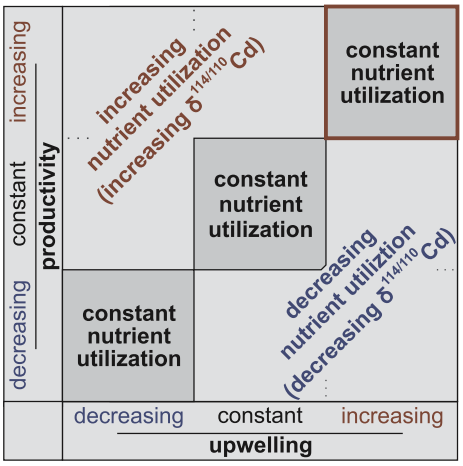

Fig. 7. Schematic cartoon illustrating the relationships between rates of upwelling (nutrient supply), productivity (nutrient demand), and nutrient utilization (fraction of the total nutrient supply consumed by demand). The combination of these three factors results in nine distinct nutrient regimes, illustrated as squares. Assuming redox conditions are favorable for Cd preservation, we constrain changes in the rates of productivity by using knowledge of changes in the rates of upwelling and changes in nutrient utilization. For the Upper Permian shales studied here, rising $\delta^{15/14}$N upsection in MNS and into GRL-LL define a regime of increasing rates of upwelling approaching the end of the Permian, supported also by increasing metal content and metal/Al ratios in the sediments. Constant $\delta^{114/110}$Cd for the same samples evidence constant nutrient utilization. Therefore, geochemical data for the studied shales preclude all scenarios except the upper-right portion of the diagram, requiring increased productivity during the Late Permian.

nitrogen utilization in oxic waters or in strongly anoxic stratified basins proceeds predominantly through pore-water denitrification, or through nitrogen fixation, respectively. Both of these mechanisms are ultimately recorded as low sedimentary $\delta^{15/14}$N. In our samples, sedimentary $\delta^{15/14}$N increases up-section in MNS and is highest in GRL-LL, suggesting an increasing strength of upwelling towards the end-Permian in MNS, and stronger upwelling in GRL compared to MNS (Fig. 6). Sustained and intensifying upwelling is also supported by the positive correlation of $\delta^{15/14}$N with [Cd] (Fig. 6a), [Mo], and Cd/Al, Zn/Al, Mo/Al and U/Al ratios (SI), as well as the concurrent enrichments of [Mo] and [Cd] in the organic-rich samples (e.g., Wagner et al., 2013).

The hypothesis that the Late Permian anoxia at GRL and MNS was caused by oceanic stagnation is not consistent with the data presented here. Considering all available proxy data, it seems likely that anoxia was instead sustained via the upwelling-productivity feedback loop (e.g., Wyrtki, 1962; Pedersen and Calvert, 1990; Fig. 5C). The data illustrate constant levels of fractional nutrient utilization as upwelling increased, as suggested by the Cd- and N-isotopic data, respectively. This situation requires increased primary productivity to balance the larger nutrient fluxes at both localities (Fig. 7). As total productivity increased, this would have favored increased OM respiration and subsequent oxygen-depletion of the water column through heterotrophy. This in turn argues against prolonged incursions of sulfidic deep waters into the surface photic zone, as this would have caused a productivity crash rather than the higher productivity, which is observed.

The above conclusion, that shallow-water anoxia developed due to higher productivity, relates only to the studied pre-extinction Upper Permian shales from the GRL-MNS shelf. Data from other sections will be needed to extrapolate this finding to the global pre-extinction Late Permian ocean, or to the global expansion of anoxic waters that may have occurred later in the Changhsingian stage at the time of mass extinction (Brennecka et al., 2011). However, a similar regime of vigorous coastal upwelling presumably existed along much of the northeastern Panthalassa margin in the pre-extinction Late Permian (e.g., Beauchamp and Baud, 2002; Schoepfer et al., 2013). High productivity has also been inferred from coupled climate-carbon numerical models for most of eastern, equatorial, and parts of the mid-latitude northwestern and southwestern Panthalassa in the Late Permian (Winguth and Winguth, 2012). Recurring upwelling also characterized shelf sections at tropical latitudes in the eastern Paleotethys (e.g., Algeo et al., 2008b). Overall, high productivity related to upwelling of nutrient-rich waters promoted oxygen depletion and global expansion of oxygen-minimum zones in the pre-extinction Late Permian, perhaps setting the stage for a more widespread and intense anoxia that reached shallow waters and caused the Late Permian mass extinction. The causes for intensifying upwelling remain speculative. Most likely, stronger upwelling was driven by tectonic reorganization that altered oceanic circulation and/or by tectonic uplift that intensified and changed direction of (local) winds, as put forward for more recent analogue settings (e.g., Jung et al., 2014).

Perhaps most importantly, our multi-isotopic geochemical data are only consistent with the upwelling-productivity feedback scenario for development and intensification of anoxia (Fig. 5C). Other possible scenarios (e.g., Figs. 5A, B) are precluded by the data, regardless of the exact mechanism of Cd delivery to the studied shales (Section 5.2). For example, it was recently proposed that CdS formation in sulfidic micro-environments of oxygen-deficient waters is one of the primary mechanisms of Cd delivery to marine sediments (Janssen et al., 2014). Our interpretations are in accord with such a scenario, even if the Cd deposition mechanisms are somewhat different. That is, increasing water column precipitation of CdS with a constant Cd-isotopic composition requires that Cd removal into micro-sulfides is balanced by the upwelling resupply of Cd from deeper waters. Without such a balance, the available Cd inventory is quickly exhausted and CdS formation would cease, causing sedimentary [Cd] to tend towards zero. The observed [Cd] increase up-section at constant $\delta^{114/110}$Cd (Fig. 1) thus requires that any CdS precipitation in the water column above GRL or MNS sections was fed by increasing upwelling. The resultant high surface productivity would have lead to substantial oxygen depletion in the water column due to OM decomposition, thereby driving more CdS precipitation. From these considerations, it is clear that the environmental conditions necessary to sustain water column CdS precipitation are essentially identical to those already required by all other sedimentary proxy data (Fig. 6). Furthermore, our metal-source term analysis strongly implicates OM as the dominant Cd carrier phase in most MNS-BS and MNS-LL samples, and does not require substantial amounts of CdS-associated authigenic Cd. Overall, these considerations highlight that our paleoenvironmental reconstruction of oxygen-deficient settings, as recorded in MNS and GRL shales, are robust, even if the exact mechanism by which Cd is deposited in certain samples remains elusive.

6. Conclusions

We show that Upper Permian organic-rich shales from Greenland and Norway were deposited during increasingly anoxic bottom water conditions. Detailed sample metal budgets show that sedimentary Cd is predominantly supplied from sinking OM, with variable authigenic enrichments, that both have equivalent Cd-isotopic compositions related to OM export. Detrital Cd contributions are insignificant in all samples. The main Cd host phase appears to be OM, with or without micro-sulfides and pyrite. All studied shales are isotopically lighter in Cd than present-day deep-ocean seawater, with a nearly constant $\delta^{114/110}$Cd of $+0.15 \pm 0.01$‰ (2 SE, $n = 12$). Using modern Cd-isotopic cycling as our interpretative framework, we suggest that the Cd-isotopic composition of Upper Permian shales reflects the open system balance

between biomass drawdown of Cd and nutrients, with constant replenishment of Cd and other nutrients from below by upwelling. As such, the Cd-isotopic composition of the underlying sediments records the extent of nutrient utilization in the surface ocean at the time of shale deposition.

Nitrogen-isotopic and trace metal/Al ratios in MNS and GRL sections suggest an intensifying upwelling regime through time. Progressive oxygen depletion of the water column was followed by development of sulfidic water column conditions prior to the Late Permian mass extinction, with a paleoredox state favoring Cd retention. The constant efficiency of nutrient utilization, with increasingly more vigorous upwelling that supplied additional nutrients to surface waters, requires enhanced paleoproductivity at both localities.

More generally, this study shows that the Cd-isotopic compositions of organic-rich shales can provide valuable information on local nutrient utilization levels in the geologic past, and, together with independent estimates for paleoredox and upwelling intensities, can also reveal changes in paleoproductivity through time.

Author contributions

HJS and JLH provided samples and conceived the project together with SVG, TJH, and MR. SVG selected, prepared, and analyzed major constituents in all samples; TJH performed Cd-isotopic analyses; and BB performed pyrite framboid analyses. SVG and TJH wrote the paper with significant contributions from MR and HJS, with editorial input from all coauthors.

Acknowledgments

We thank Gideon M. Henderson for providing access to lab facilities at the University of Oxford. Viebeke Hatlø and Elin Rein (Statoil ASA) provided Rock–Eval data. Stefan Piasecki provided samples from GEUS core in GRL. This work was supported by the CHRONOS project in collaboration with CEED-UiO (HJS, JLH), and the Petromaks project 180015/S30 (HJS, JLH, BB). TJH was supported by NERC Doctoral Training Grant NE/G524060/1 and Nu Instruments. We greatly appreciate the constructive and in-depth comments by two anonymous reviewers, which improved the quality of the manuscript, and acknowledge editorial handling by Jean Lynch-Stieglitz.

Appendix A. Supplementary material

Supplementary material related to this article can be found online at http://dx.doi.org/10.1016/j.epsl.2014.11.010.

References

Abouchami, W., Galer, S.J.G., de Baar, H.J.W., Alderkamp, A.C., Middag, R., Laan, P., Feldmann, H., Andreae, M.O., 2011. Modulation of the Southern Ocean cadmium isotope signature by ocean circulation and primary productivity. Earth Planet. Sci. Lett. 305 (1–2), 83–91.

Abouchami, W., Galer, S.J.G., Horner, T.J., Rehkämper, M., Wombacher, F., Xue, Z.C., Lambelet, M., Gault-Ringold, M., Stirling, C.H., Schönbächler, M., Shiel, A.E., Weis, D., Holdship, P.F., 2012. A common reference material for cadmium isotope studies – NIST SRM 3108. Geostand. Geoanal. Res. 37 (1), 5–17.

Abouchami, W., Galer, S.J.G., de Baar, H.J.W., Middag, R., Vance, D., Zhao, Y., Klunder, M., Mezger, K., Feldmann, H., Andreae, M.O., 2014. Biogeochemical cycling of cadmium isotopes in the Southern Ocean along the Zero Meridian. Geochim. Cosmochim. Acta 127, 348–367.

Algeo, T.J., Lyons, T.W., 2006. Mo-total organic carbon covariation in modern anoxic marine environments: implications for analysis of paleoredox and paleohydrographic conditions. Paleoceanography 21 (1), 1016.

Algeo, T., Rowe, H., Hower, J.C., Schwark, L., Herrmann, A., Heckel, P., 2008a. Changes in ocean denitrification during Late Carboniferous glacial–interglacial cycles. Nat. Geosci. 1 (10), 709–714.

Algeo, T., Shen, Y.A., Zhang, T.G., Lyons, T., Bates, S., Rowe, H., Nguyen, T.K.T., 2008b. Association of ^{34}S-depleted pyrite layers with negative carbonate δ^{13}C excursions at the Permian–Triassic boundary: evidence for upwelling of sulfidic deep-ocean water masses. Geochem. Geophys. Geosyst. 9, Q04025. http://dx.doi.org/10.1029/2007GC001823.

Algeo, T.J., Hinnov, L., Moser, J., Maynard, J.B., Elswick, E., Kuwahara, K., Sano, H., 2010. Changes in productivity and redox conditions in the Panthalassic Ocean during the latest Permian. Geology 38 (2), 187–190.

Beauchamp, B., Baud, A., 2002. Growth and demise of Permian biogenic chert along northwest Pangea: evidence for end-Permian collapse of thermohaline circulation. Palaeogeogr. Palaeoclimatol. Palaeoecol. 184 (1–2), 37–63.

Berner, R.A., Raiswell, R., 1983. Burial of organic carbon and pyrite sulfur in sediments over Phanerozoic time – a new theory. Geochim. Cosmochim. Acta 47 (5), 855–862.

Bond, D.P.G., Wignall, P.B., 2010. Pyrite framboid study of marine Permian–Triassic boundary sections: a complex anoxic event and its relationship to contemporaneous mass extinction. Bull. Geol. Soc. Am. 122 (7–8), 1265–1279.

Böning, P., Brumsack, H.J., Böttcher, M.E., Schnetger, B., Kriete, C., Kallmeyer, J., Borchers, S.L., 2004. Geochemistry of Peruvian near-surface sediments. Geochim. Cosmochim. Acta 68 (21), 4429–4451.

Boyle, E.A., 1988. Cadmium: chemical tracer of deepwater paleoceanography. Paleoceanography 3 (4), 471–489.

Boyle, E.A., Sclater, F., Edmond, J.M., 1976. On the marine geochemistry of cadmium. Nature 263 (5572), 42–44.

Brennecka, G.A., Herrmann, A.D., Algeo, T.J., Anbar, A.D., 2011. Rapid expansion of oceanic anoxia immediately before the end-Permian mass extinction. Proc. Natl. Acad. Sci. USA 108 (43), 17631–17634.

Bruland, K.W., 1980. Oceanographic distributions of cadmium, zinc, nickel, and copper in the North Pacific. Earth Planet. Sci. Lett. 47 (2), 176–198.

Brumsack, H.J., 2006. The trace metal content of recent organic carbon-rich sediments: implications for Cretaceous black shale formation. Palaeogeogr. Palaeoclimatol. Palaeoecol. 232 (2–4), 344–361.

Bugge, T., Ringås, J.E., Leith, D.A., Mangerud, G., Weiss, H.M., Leith, T.L., 2002. Upper Permian as a new play model on the mid-Norwegian continental shelf: investigated by shallow stratigraphic drilling. Am. Assoc. Pet. Geol. Bull. 86 (1), 107–127.

Burgess, S.D., Bowring, S., Shen, S.Z., 2014. High-precision timeline for Earth's most severe extinction. Proc. Natl. Acad. Sci. USA 111 (9), 3316–3321.

Chappaz, A., Lyons, T.W., Gregory, D.D., Reinhard, C.T., Gill, B.C., Li, C., Large, R.R., 2014. Does pyrite act as an important host for molybdenum in modern and ancient euxinic sediments? Geochim. Cosmochim. Acta 126, 112–122.

Conway, T.M., Rosenberg, A.D., Adkins, J.F., John, S.G., 2013. A new method for precise determination of iron, zinc and cadmium stable isotope ratios in seawater by double-spike mass spectrometry. Anal. Chim. Acta 793, 44–52.

Cornford, C., 1998. Source rocks and hydrocarbons of the North Sea. In: Glennie, K.W. (Ed.), Petroleum Geology of the North Sea. Blackwell Science Publications, Oxford, UK, pp. 376–462.

Cornford, C., Burgess, C., Gliddon, T., Kelly, R., 2001. Geochemical truths in large data sets – II: risking petroleum systems. In: 20th International Meeting on Organic Geochemistry. Nancy, France, pp. 322–323.

Crusius, J., Calvert, S., Pedersen, T., Sage, D., 1996. Rhenium and molybdenum enrichments in sediments as indicators of oxic, suboxic and sulfidic conditions of deposition. Earth Planet. Sci. Lett. 145 (1–4), 65–78.

Cullen, J.T., 2006. On the nonlinear relationship between dissolved cadmium and phosphate in the modern global ocean: could chronic iron limitation of phytoplankton growth cause the kink? Limnol. Oceanogr. 51 (3), 1369–1380.

Elderfield, H., McCaffrey, R.J., Luedtke, N., Bender, M., Truesdale, V.W., 1981. Chemical diagenesis in Narragansett bay sediments. Am. J. Sci. 281 (8), 1021–1055.

Espitalié, J., Madec, M., Tissot, B., 1980. Role of mineral matrix in kerogen pyrolysis – influence on petroleum generation and migration. Am. Assoc. Pet. Geol. Bull. 64 (1), 59–66.

Framson, P.E., Leckie, J.O., 1978. Limits of coprecipitation of cadmium and ferrous sulfides. Environ. Sci. Technol. 12 (4), 465–469.

Georgiev, S., Stein, H.J., Hannah, J.L., Bingen, B., Weiss, H.M., Piasecki, S., 2011. Hot acidic Late Permian seas stifle life in record time. Earth Planet. Sci. Lett. 310 (3–4), 389–400.

Georgiev, S., Stein, H.J., Hannah, J.L., Weiss, H.M., Bingen, B., Xu, G.P., Rein, E., Hatlø, V., Løseth, H., Nali, M., Piasecki, S., 2012. Chemical signals for oxidative weathering predict Re–Os isochroneity in black shales, East Greenland. Chem. Geol. 324, 108–121.

Gobeil, C., Silverberg, N., Sundby, B., Cossa, D., 1987. Cadmium diagenesis in Laurentian Trough sediments. Geochim. Cosmochim. Acta 51 (3), 589–596.

Gobeil, C., MacDonald, R.W., Sundby, B., 1997. Diagenetic separation of cadmium and manganese in suboxic continental margin sediments. Geochim. Cosmochim. Acta 61 (21), 4647–4654.

Helz, G.R., Miller, C.V., Charnock, J.M., Mosselmans, J.F.W., Pattrick, R.A.D., Garner, C.D., Vaughan, D.J., 1996. Mechanism of molybdenum removal from the sea and its concentration in black shales: EXAFS evidence. Geochim. Cosmochim. Acta 60 (19), 3631–3642.

Henderson, C.M., Mei, S., 2000. Preliminary cool water Permian conodont zonation in North Pangea: a review. Permophiles 36, 16–23.

Hendry, K.R., Rickaby, R.E.M., de Hoog, J.C.M., Weston, K., Rehkämper, M., 2008. Cadmium and phosphate in coastal Antarctic seawater: implications for Southern Ocean nutrient cycling. Mar. Chem. 112 (3–4), 149–157.
Ho, T.Y., Quigg, A., Finkel, Z.V., Milligan, A.J., Wyman, K., Falkowski, P.G., Morel, F.M.M., 2003. The elemental composition of some marine phytoplankton. J. Phycol. 39 (6), 1145–1159.
Horner, T.J., Rickaby, R.E.M., Henderson, G.M., 2011. Isotopic fractionation of cadmium into calcite. Earth Planet. Sci. Lett. 312 (1–2), 243–253.
Horner, T.J., Lee, R.B.Y., Henderson, G.M., Rickaby, R.E.M., 2013. Nonspecific uptake and homeostasis drive the oceanic cadmium cycle. Proc. Natl. Acad. Sci. USA 110 (7), 2500–2505.
Huerta-Diaz, M.A., Morse, J.W., 1992. Pyritization of trace metals in anoxic marine sediments. Geochim. Cosmochim. Acta 56 (7), 2681–2702.
Hunt, J.M., 1995. Petroleum Geochemistry and Geology. W.H. Freeman and Company, New York, 743 pp.
Isozaki, Y., 1997. Permo-Triassic boundary superanoxia and stratified superocean: records from lost deep sea. Science 276 (5310), 235–238.
Janssen, D.J., Conway, T.M., John, S.G., Christian, J.R., Kramer, D.I., Pedersen, T.F., Cullen, J.T., 2014. Undocumented water column sink for cadmium in open ocean oxygen-deficient zones. Proc. Natl. Acad. Sci. USA 111 (19), 6888–6893.
Jenkyns, H.C., Gröcke, D.R., Hesselbo, S.P., 2001. Nitrogen isotope evidence for water mass denitrification during the early Toarcian (Jurassic) oceanic anoxic event. Paleoceanography 16 (6), 593–603.
John, S.G., Conway, T.M., 2014. A role for scavenging in the marine biogeochemical cycling of zinc and zinc isotopes. Earth Planet. Sci. Lett. 394, 159–167.
Jorgensen, B.B., 1982. Mineralization of organic matter in the sea bed – the role of sulfate reduction. Nature 296 (5858), 643–645.
Jung, G., Prange, M., Schulz, M., 2014. Uplift of Africa as a potential cause for Neogene intensification of the Benguela upwelling system. Nat. Geosci. 1 (10), 741–747.
Lacan, F., Francois, R., Ji, Y.C., Sherrell, R.M., 2006. Cadmium isotopic composition in the ocean. Geochim. Cosmochim. Acta 70 (20), 5104–5118.
Lane, T.W., Saito, M.A., George, G.N., Pickering, I.J., Prince, R.C., Morel, F.M.M., 2005. A cadmium enzyme from a marine diatom. Nature 435 (7038), 42.
Large, R.R., Halpin, J.A., Danyushevsky, L.V., Maslennikov, V.V., Bull, S.W., Long, J.A., Gregory, D.D., Lounejeva, E., Lyons, T.W., Sackj, P.J., McGoldrick, P.J., Calver, C.R., 2014. Trace element content of sedimentary pyrite as a new proxy for deep-time ocean–atmosphere evolution. Earth Planet. Sci. Lett. 389, 209–220.
Marchitto, T.M., Broecker, W.S., 2006. Deep water mass geometry in the glacial Atlantic Ocean: a review of constraints from the paleonutrient proxy Cd/Ca. Geochem. Geophys. Geosyst. 7, Q12003. http://dx.doi.org/10.1029/2006GC001323.
Martin, J.M., Thomas, A.J., 1994. The global insignificance of telluric input of dissolved trace metals (Cd, Cu, Ni and Zn) to ocean margins. Mar. Chem. 46 (1–2), 165–178.
McCorkle, D.C., Klinkhammer, G.P., 1991. Porewater cadmium geochemistry and the porewater cadmium: δ^{13}C relationship. Geochim. Cosmochim. Acta 55 (1), 161–168.
Meyer, K.M., Yu, M., Jost, A.B., Kelley, B.M., Payne, J.L., 2011. δ^{13}C evidence that high primary productivity delayed recovery from end-Permian mass extinction. Earth Planet. Sci. Lett. 302 (3–4), 378–384.
Morford, J.L., Emerson, S., 1999. The geochemistry of redox sensitive trace metals in sediments. Geochim. Cosmochim. Acta 63 (11–12), 1735–1750.
Nameroff, T.J., Balistrieri, L.S., Murray, J.W., 2002. Suboxic trace metal geochemistry in the eastern tropical North Pacific. Geochim. Cosmochim. Acta 66 (7), 1139–1158.
Nielsen, J.K., Shen, Y., 2004. Evidence for sulfidic deep water during the Late Permian in the East Greenland Basin. Geology 32, 1037–1040.
Parnell, J., Still, J., Spinks, S., Thayalan, W., Bowden, S., 2014. Cadmium sulfide in a Mesoproterozoic terrestrial environment. Mineral. Mag. 78 (1), 47–54.
Pedersen, T.F., Calvert, S.E., 1990. Anoxia vs productivity – what controls the formation of organic-carbon-rich sediments and sedimentary rocks. Am. Assoc. Pet. Geol. Bull. 74 (4), 454–466.
Pedersen, T.F., Waters, R.D., Macdonald, R.W., 1989. On the natural enrichment of cadmium and molybdenum in the sediments of Ucluelet Inlet, British Columbia. Sci. Total Environ. 79 (2), 125–139.
Peters, K.E., 1986. Guidelines for evaluating petroleum source rock using programmed pyrolysis. Am. Assoc. Pet. Geol. Bull. 70 (3), 318–329.
Piasecki, S., Stemmerik, L., 1991. Late Permian anoxia in central East Greenland. In: Tyson, R.V., Pearson, T.H. (Eds.), Modern and Ancient Continental Shelf Anoxia. In: Geol. Soc. (Lond.) Spec. Publ., pp. 275–290.
Pinet, P.R., 2011. Invitation to Oceanography. Jones & Bartlett Publishers, 620 pp.
Quan, T.M., Wright, J.D., Falkowski, P.G., 2013. Co-variation of nitrogen isotopes and redox states through glacial–interglacial cycles in the Black Sea. Geochim. Cosmochim. Acta 112, 305–320.
Redfield, A.C., 1934. On the proportions of organic derivatives in sea water and their relation to the composition of plankton. In: James Johnstone Memorial Volume. University Press of Liverpool, 176 pp.
Rehkämper, M., Wombacher, F., Horner, T.J., Xue, Z., 2011. Natural and anthropogenic Cd isotope variations. In: Baskaran, M. (Ed.), Handbook of Environmental Isotope Geochemistry. Advances in Isotope Geochemistry. Springer-Verlag, Berlin, Heidelberg, pp. 125–154.
Ripperger, S., Rehkämper, M., Porcelli, D., Halliday, A.N., 2007. Cadmium isotope fractionation in seawater – a signature of biological activity. Earth Planet. Sci. Lett. 261 (3–4), 670–684.
Rosenthal, Y., Lam, P., Boyle, E.A., Thomson, J., 1995. Authigenic cadmium enrichments in suboxic sediments – precipitation and postdepositional mobility. Earth Planet. Sci. Lett. 132 (1–4), 99–111.
Rudnick, P.L., Gao, S., 2004. Composition of the continental crust. In: Holland, H.D., Turekian, K.K. (Eds.), Treatise on Geochemistry. Elsevier, Amsterdam, pp. 1–64.
Schmitt, A.D., Galer, S.J.G., Abouchami, W., 2009. Mass-dependent cadmium isotopic variations in nature with emphasis on the marine environment. Earth Planet. Sci. Lett. 277 (1–2), 262–272.
Schoepfer, S.D., Henderson, C.M., Garrison, G.H., Foriel, J., Ward, P.D., Selby, D., Hower, J.C., Algeo, T.J., Shen, Y., 2013. Termination of a continent-margin upwelling system at the Permian–Triassic boundary (Opal Creek, Alberta, Canada). Glob. Planet. Change 105, 21–35.
Selby, D., Creaser, R.A., 2003. Re–Os geochronology of organic rich sediments: an evaluation of organic matter analysis methods. Chem. Geol. 200 (3–4), 225–240.
Sengör, A.M.C., Atayman, S., 2009. The Permian extinction and the Tethys: an exercise in global geology. Spec. Pap., Geol. Soc. Am. 448, 1–85.
Stemmerik, L., Bendix-Almgreen, S.E., Piasecki, S., 2001. The Permian–Triassic boundary in central East Greenland: past and present views. Bull. Geol. Soc. Denmark 48, 159–167.
Sunda, W.G., 2012. Feedback interactions between trace metal nutrients and phytoplankton in the ocean. Frontiers Microbiol. 3.
Sundby, B., Martinez, P., Gobeil, C., 2004. Comparative geochemistry of cadmium, rhenium, uranium, and molybdenum in continental margin sediments. Geochim. Cosmochim. Acta 68 (11), 2485–2493.
Surlyk, F., Hurst, J.M., Piasecki, S., Rolle, F., Scholle, P.A., Stemmerik, L., Thomsen, E., 1986. The Permian of the western margin of the Greenland Sea – a future exploration target. In: Halbouty, M.T. (Ed.), Future Petroleum Provinces of the World. AAPG Memoir, pp. 629–659.
Torsvik, T.H., Carlos, D., Mosar, J., Cocks, L.R.M., Malme, T.N., 2002. Global reconstructions and North Atlantic paleogeography 440 Ma to Recent. In: Eide, E.A. (Ed.), BATLAS – Mid Norway Plate Reconstruction Atlas with Global and Atlantic Perspectives. Geological Survey of Norway, Trondheim, pp. 18–39.
Turekian, K.K., Wedepohl, K.H., 1961. Distribution of the elements in some major units of the Earth's crust. Bull. Geol. Soc. Am. 72 (2), 175–191.
Turgeon, S., Brumsack, H.J., 2006. Anoxic vs dysoxic events reflected in sediment geochemistry during the Cenomanian–Turonian Boundary Event (Cretaceous) in the Umbria–Marche Basin of central Italy. Chem. Geol. 234 (3–4), 321–339.
van Geen, A., McCorkle, D.C., Klinkhammer, G.P., 1995. Sensitivity of the phosphate–cadmium–carbon isotope relation in the ocean to cadmium removal by suboxic sediments. Paleoceanography 10 (2), 159–169.
Wagner, M., Hendy, I.L., McKay, J.L., Pedersen, T.F., 2013. Influence of biological productivity on silver and redox-sensitive trace metal accumulation in Southern Ocean surface sediments, Pacific sector. Earth Planet. Sci. Lett. 380, 31–40.
Wedepohl, K.H., 1995. The composition of the continental crust. Geochim. Cosmochim. Acta 59 (7), 1217–1232.
Wignall, P.B., Twitchett, R.J., 2002a. Extent, duration, and nature of the Permian–Triassic superanoxic event. Spec. Pap., Geol. Soc. Am. 356, 395–413.
Wignall, P.B., Twitchett, R.J., 2002b. Permian–Triassic sedimentology of Jameson Land, East Greenland: incised submarine channels in an anoxic basin. J. Geol. Soc. 159, 691–703.
Wilkin, R.T., Barnes, H.L., Brantley, S.L., 1996. The size distribution of framboidal pyrite in modern sediments: an indicator of redox conditions. Geochim. Cosmochim. Acta 60 (20), 3897–3912.
Winguth, C., Winguth, A.M.E., 2012. Simulating Permian–Triassic oceanic anoxia distribution: implications for species extinction and recovery. Geology 40 (2), 127–130.
Wombacher, F., Rehkämper, M., Mezger, K., Munker, C., 2003. Stable isotope compositions of cadmium in geological materials and meteorites determined by multiple-collector ICPMS. Geochim. Cosmochim. Acta 67 (23), 4639–4654.
Wyrtki, K., 1962. The oxygen minima in relation to ocean circulation. Deep-Sea Res. 9 (1), 11–23.
Xu, G.P., Hannah, J.L., Bingen, B., Georgiev, S., Stein, H.J., 2012. Digestion methods for trace element measurements in shales: paleoredox proxies examined. Chem. Geol. 324, 132–147.
Xue, Z.C., Rehkämper, M., Schönbächler, M., Statham, P.J., Coles, B.J., 2012. A new methodology for precise cadmium isotope analyses of seawater. Anal. Bioanal. Chem. 402 (2), 883–893.
Xue, Z.C., Rehkämper, M., Horner, T.J., Abouchami, W., Middag, R., van de Flierd, T., de Baar, H.J.W., 2013. Cadmium isotope variations in the Southern Ocean. Earth Planet. Sci. Lett. 382, 161–172.